

Semiconducting Polymer Nanoparticles for Centimeters-Deep Photoacoustic Imaging in the Second Near-Infrared Window

Jiayingzi Wu, Liyan You, Lu Lan, Hyeon Jeong Lee, Saadia T. Chaudhry, Rui Li, Ji-Xin Cheng,* and Jianguo Mei*

Thienoisindigo-based semiconducting polymer with a strong near-infrared absorbance is synthesized and its water-dispersed nanoparticles (TSPNs) are investigated as a contrast agent for photoacoustic (PA) imaging in the second near-infrared (NIR-II) window (1000–1350 nm). The TSPNs generate a strong PA signal in the NIR-II optical window, where background signals from endogenous contrast agents, including blood and lipid, are at the local minima. By embedding a TSPN-containing tube in chicken-breast tissue, an imaging depth of more than 5 cm at 1064 nm excitation is achieved with a contrast-agent concentration as low as 40 $\mu\text{g mL}^{-1}$. The TSPNs under the skin or in the tumor are clearly visualized at 1100 and 1300 nm, with negligible interference from the tissue background. TSPN as a PA contrast in the NIR-II window opens new opportunities for biomedical imaging of deep tissues with improved contrast.

Noninvasive imaging of targets in centimeter-deep tissues is important for preclinical and clinical studies of physiological and pathogenic processes, which could make diagnosis and/or treatments more effective and efficient.^[1–4] Among the various modalities for deep-tissue imaging, photoacoustic (PA) imaging is an emerging hybrid approach, which combines optical excitation and ultrasonic detection. Compared to traditional optical techniques, PA imaging provides a deeper penetration and higher spatial resolution, while maintaining rich contrast and high sensitivity.^[5–7] Although the penetration depth in PA imaging is significantly improved due to the low acoustic scattering in biological tissue (three orders of magnitude less

than optical scattering) and high optical absorption sensitivity (two orders of magnitude greater than those of confocal microscopy and optical coherence tomography),^[4] it is still limited by the attenuation of excitation light on account of optical absorption and scattering.^[8] In addition, the optical absorption of blood and other biological compounds from tissue reduces the imaging contrast and sensitivity. To address these challenges, efforts have been devoted to developing exogenous contrast agents with absorption in the second near-infrared (NIR-II) window (1000–1350 nm),^[9–15] where light scattering is decreased and absorption of blood and other biological compounds is minimized.^[16,17]

Semiconducting polymer nanoparticles (SPNs) represent a new class of PA contrast agents with good biocompatibility as organic compounds,^[18] excellent photostability, high mass extinction, and controllable dimensions.^[19] SPNs have been used for in vivo PA imaging of tumors,^[20] reactive oxygen species,^[19,21,22] and pH^[23] in the first near-infrared (NIR-I) window (650–950 nm).^[24] Thus far, SPNs for PA imaging in the NIR-II region have seldom been reported.^[25] Here, we report a completely new SPN system, thienoisindigo (TII)-based semiconducting polymer nanoparticles (TSPNs), with strong absorption in 1000–1350 nm for PA imaging in the NIR-II window. TII, an electron-deficient unit with high planarity, was previously developed for applications in organic electronics.^[26] TII homopolymers have displayed an ultranarrow bandgap with strong absorption in the NIR-II window.^[27,28] We designed and synthesized new TII-based semiconducting polymers with triethylene glycol (TEG) side-chains (TII-TEG), and then formulated them into TSPNs. Next, we characterized the PA properties of TSPN in vitro, and measured the penetration depth in chicken-breast tissue. Last, we demonstrated the potential of TSPN for skin and tumor imaging in vivo.

The synthesis of TII-TEG is shown in **Figure 1a**. The highly planar backbone contributes to a long absorption wavelength in the NIR-II region.^[27] Additionally, to further enhance the biocompatibility of the exogenous contrast agent, TEG-side chains were attached to the polymer backbones.^[29] Stable TSPNs (**Figure 1b**) in aqueous solutions were formulated through the nanoprecipitation method, where a tetrahydrofuran (THF) solution

J. Wu, L. You, S. T. Chaudhry, Prof. J.-X. Cheng, Prof. J. Mei
Department of Chemistry
Purdue University
West Lafayette, IN 47907, USA
E-mail: jcheng@purdue.edu; jgmei@purdue.edu

L. Lan, H. J. Lee, R. Li, Prof. J.-X. Cheng
Weldon School of Biomedical Engineering
Purdue University
West Lafayette, IN 47907, USA

H. J. Lee
Interdisciplinary Life Science Program
Purdue University
West Lafayette, IN 47907, USA

 The ORCID identification number(s) for the author(s) of this article can be found under <https://doi.org/10.1002/adma.201703403>.

DOI: 10.1002/adma.201703403

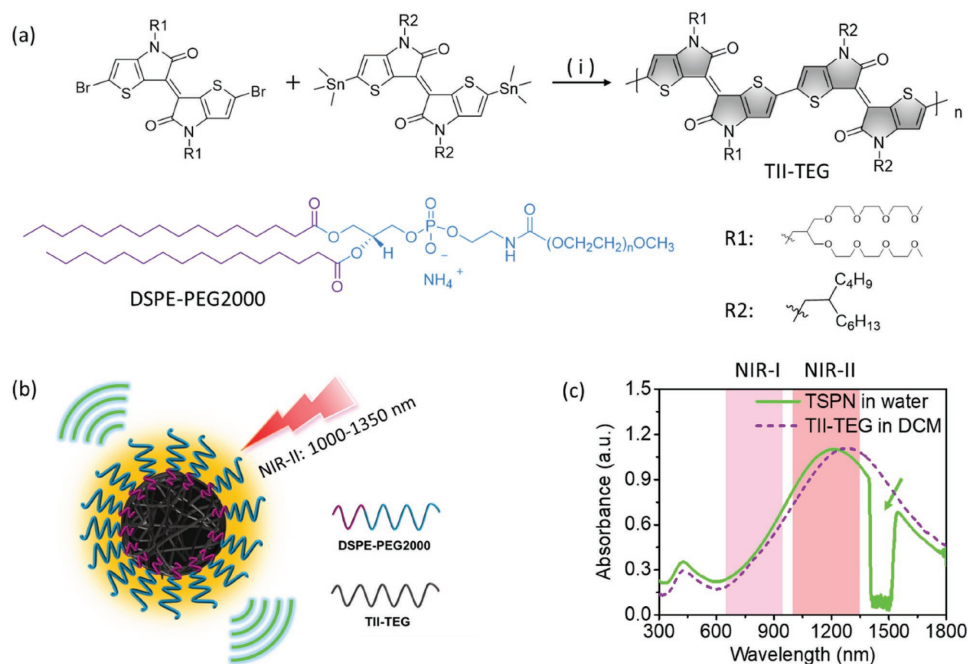


Figure 1. Preparation and absorption of TSPN: a) Synthetic route of TII-TEG. i) P(o-toly), Pd₂(dba)₃, toluene, 110 °C. Chemical structure of DSPE-PEG2000. b) Schematic illustration of TSPN prepared by nanoprecipitation. c) Absorption spectra of TSPN in water (solid green line) and TII-TEG in dichloromethane (DCM) (dashed purple line). The convex in the curve of the aqueous solution resulted from the absorption saturation of water.

containing TII-TEG and 1,2-dipalmitoyl-*sn*-glycero-3-phosphoethanolamine-N-[methoxy[poly(ethylene glycol)]-2000] (DSPE-PEG2000) was quickly injected into water under sonication. THF was then removed by the nitrogen bubbling method. The resulted TSPNs exhibited broad absorption that covers both NIR-I and NIR-II regions (Figure 1c). The convex in the absorption spectrum of the TSPN aqueous solution resulted from the absorption saturation of water, and more discussions can be found in the Supporting Information (Figure S1 and S2, Supporting Information). In particular, its corresponding mass extinction coefficient in water at 1200 nm was $35 \pm 5 \text{ mL mg}^{-1} \text{ cm}^{-1}$, which is comparable to that of NIR dyes (indocyanine green) at 800 nm ($126.6 \text{ mL mg}^{-1} \text{ cm}^{-1}$ ($98 \text{ 148 M}^{-1} \text{ cm}^{-1}$), with a concentration of $7.75 \mu\text{g mL}^{-1}$ ($9.01 \times 10^{-3} \text{ M}$)),^[30] as well as that of diketopyrrolopyrrole-based SPNs at 748 nm ($76 \text{ mL mg}^{-1} \text{ cm}^{-1}$).^[20]

The number-averaged size of TSPNs in an aqueous solution was characterized via dynamic light scattering (DLS) and was estimated to be $86 \pm 11 \text{ nm}$ (Figure 2a), which is within the desirable size range of enhanced permeability and retention effect for passive targeted drug delivery in the next stage.^[31,32] No change in size was observed after 50 days, indicating the excellent aqueous stability. The spherical structure of TSPNs was further confirmed by transmission electron microscopy (Figure S3, Supporting Information). To investigate the biocompatibility of TSPN, we carried out cytotoxicity tests using various human cell lines (Figure S4, Supporting Information). No overt toxicity was found after incubation with TSPNs at concentrations up to $40 \mu\text{g mL}^{-1}$. Thus, the $40 \mu\text{g mL}^{-1}$ concentration was used in the following experiments.

As shown in Figure 2b, TSPN generated a strong PA signal over the entire NIR-II region, which is consistent with its

absorption spectrum (Figure 1c). For comparison of TSPN with the major endogenous contrast agents, the PA spectra of pure olive oil (a representative of lipid), water, and hemoglobin (Hb) (50 mg mL^{-1})^[33] were obtained. The PA signal of olive oil was dominant at 1210 nm with two local minima at ≈ 1100 and $\approx 1300 \text{ nm}$. The PA signal intensity of Hb was relatively large at 1000 nm but continuously decreased at longer wavelengths. On the contrary, the PA signal intensity of water gradually increased after 1100 nm, and became remarkable at $\approx 1400 \text{ nm}$. Overall, the background signals from Hb, olive oil, and water reached minima at ≈ 1100 and $\approx 1300 \text{ nm}$. Thus, by using TSPN with high PA intensity in the entire NIR-II region, the optimal contrast could be achieved at ≈ 1100 and $\approx 1300 \text{ nm}$. It is worth noting that the PA intensity of Hb was ≈ 3.8 times lower at 1300 nm than that at 1100 nm. Therefore, PA imaging at 1300 nm is expected to provide excellent contrast in blood-rich tissues such as liver, kidney, lungs, heart, and spleen.

To further validate the spectroscopy data, we performed PA imaging of above-mentioned compounds. Three transparent plastic (polyurethane) tubes containing TSPN solution, whole blood, and olive oil were implanted in an agar gel. In Figure 2c, the blood was clearly visualized at 1000 nm, but became much less visible at 1100 nm and almost invisible at 1300 nm. For olive oil, the contrast was only apparent at 1200 nm. On the other hand, TSPN maintained a high brightness from 1000 to 1300 nm. The intensity values for each tube from the images were extracted for quantitative comparison, and the derived curves (wavelength vs PA intensities) are consistent with the PA spectra results (Figure S6, Supporting Information). All signal intensities were normalized with the excitation laser energy density at different wavelengths unless otherwise mentioned, mainly because the optical attenuation in the acoustic coupling

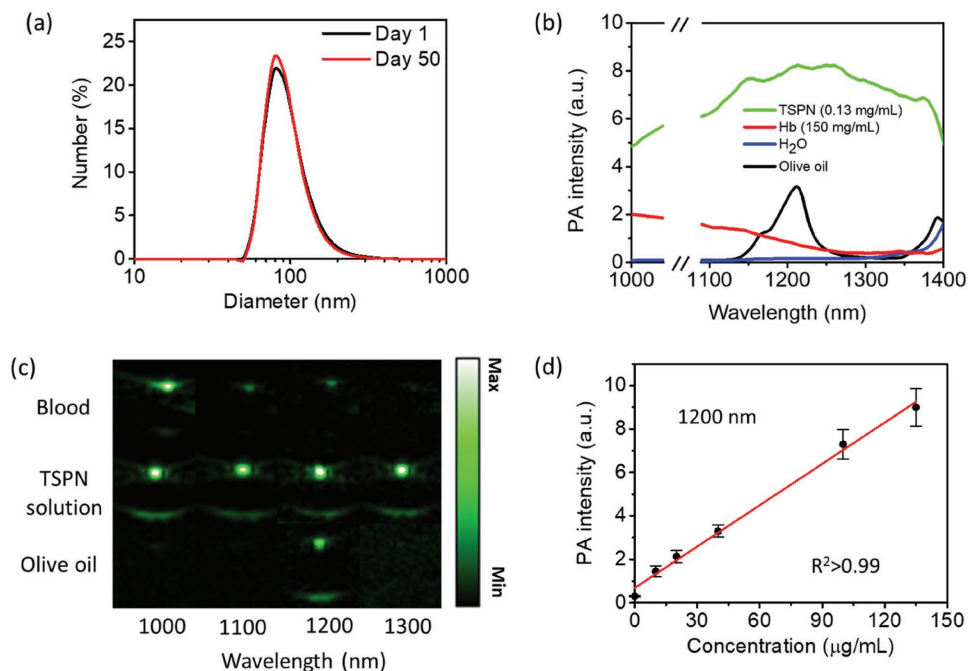


Figure 2. a) Representative DLS profiles on the first day when the TSPN solution was freshly prepared (black line) and on the fiftieth day (red line). PA properties of TSPN: b) PA spectra of water (H₂O), 150 mg mL⁻¹ hemoglobin (Hb), lipid (represented by olive oil), and 1.3 mg mL⁻¹ TSPNs. The spectra of TSPN and Hb were obtained by subtraction of water from the spectra of TSPN and Hb aqueous solutions, respectively. c) PA images of blood, 40 μg mL⁻¹ TSPNs, and lipid (represented by olive oil) contained in transparent plastic tubes with a laser wavelength at 1000, 1100, 1200, and 1300 nm, respectively. d) PA intensity of TSPN at 1200 nm as a function of mass concentration. $R^2 > 0.99$. Error bars represent for standard deviations.

media at each wavelength is different. Notably, the absorption coefficient of water, the major absorber in acoustic coupling media, is one-order of magnitude lower at 1100 nm than that at 1200 or 1300 nm.^[34] This presents one of the advantages of using 1100 nm instead of 1300 nm for excitation.

Next, the photoacoustic signal properties of TSPN were further characterized. In PA microscope spectroscopy, the PA signal intensity at NIR-II wavelengths remained stable over excitation by 12 000 pulses at the energy level of $\approx 45 \mu\text{J}$ ($\approx 1 \text{ J cm}^{-2}$ at the focus), showing good photostability of TSPN (Figure S7, Supporting Information). The PA intensities of TSPNs at 1200 nm were determined at different concentrations, displaying a linear relationship between PA signal intensity and concentration (Figure 2d). Under the same experimental condition, the detection sensitivity, defined as 1:1 signal to background ratio, was estimated to be $\approx 3 \mu\text{g mL}^{-1}$.

To explore the potential of TSPN for the deep-tissue imaging, we assessed the PA imaging depth at 1064 nm using chicken-breast tissue as a scattering medium. A transmission-mode detection was adopted in this experiment. To be analogous to a reflection-mode, we placed the same thicknesses of chicken-breast tissues below and above a transparent plastic tube filled with TSPN solution, so that the excitation light and ultrasound (US) traveled the same distance within the tissue (Figure 3a). The PA images at different depths were collected by changing the number of layers of chicken-breast tissues below and above the tube simultaneously. The corresponding laser energy density was $\approx 55 \text{ mJ cm}^{-2}$ and 100 images were acquired and averaged at the same position. The signal-to-noise ratio (SNR) of PA signal was plotted as a function of depth and was fitted

into an exponential function based on Lambert–Beer’s law (Figure 3b).^[35,36] The optical effective attenuation coefficient (defined as the slope of the fitted curve) was calculated to be 1.26 cm^{-1} , corresponding to 0.79 cm optical penetration depth. Notably, the tube containing 40 μg mL⁻¹ TSPNs was clearly visualized up to 5.3 cm with a SNR of 82 (Figure 3c). As a result, the achieved imaging depth is 6.7 times larger than the optical penetration depth. Furthermore, the imaging-depth limit was calculated to be 6.3 cm by extending the fitted curve to where the SNR of TSPNs was equivalent to the SNR of tissue background (SNR = 20). Compared to NIR-II copper sulfide quantum dots,^[10] 2.5 times less mass concentration of TSPNs is required to reach the same imaging depth of $\approx 5 \text{ cm}$ at 1064 nm, and with only half of the laser energy density. To the best of our knowledge, the current record of PA imaging depth is 11.6 cm by using phthalocyanines,^[11] but the mass concentration ($\approx 50\,000 \mu\text{g mL}^{-1}$ ($30 \times 10^{-3} \text{ M}$)) is ≈ 1250 times higher than that of TSPNs in this work. These data collectively show that TSPN is a competitive NIR-II contrast agent for centimeters-deep PA imaging.

After characterizing the PA properties of TSPN in vitro in agar gels and ex vivo in chicken-breast tissues, we further evaluated the performance of TSPN in living subjects by subcutaneous injection of matrigel-containing solutions of TSPNs (50 μL, 40 μg mL⁻¹) into the dorsal area of rats. As shown in Figure 4a, for a skin tissue without injection, the lowest signal was observed at 1300 nm, possibly due to the least intrinsic blood absorption, and the signal at 1100 nm was comparably weak. In the meantime, the stronger absorptions of blood at 800 and 1000 nm led to the higher PA signal intensities at

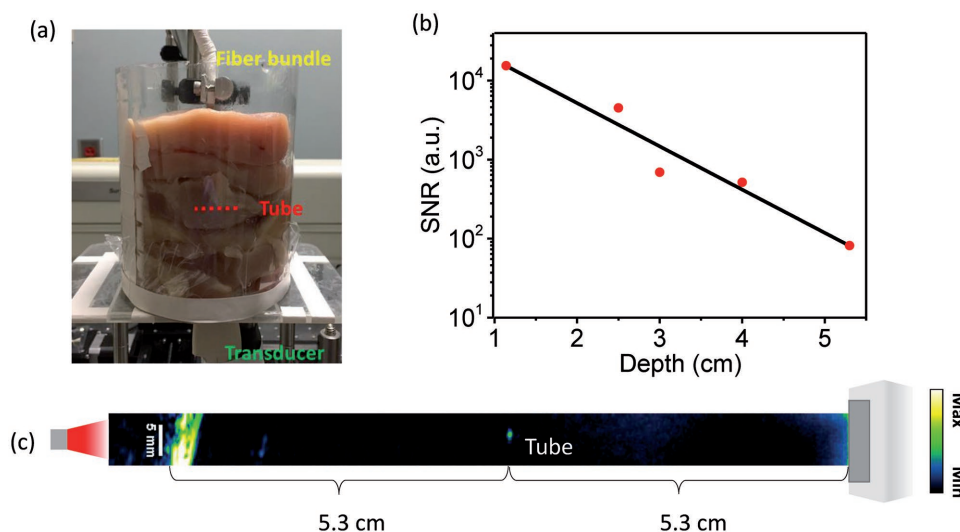


Figure 3. PA imaging of TSPN embedded in a chicken-breast tissue. a) Photograph of the experimental setup. The tube was placed in the middle of chicken-breast tissue layers. b) SNR of $40 \mu\text{g mL}^{-1}$ TSPNs contained in a transparent plastic tube as a function of depth from illuminated tissue surface with a laser wavelength at 1064 nm. c) PA image of the $40 \mu\text{g mL}^{-1}$ TSPNs in a transparent plastic tube at 5.3 cm depth. Laser energy density was tuned to 55 mJ cm^{-2} .

these wavelengths. The strong signal at 1200 nm was generated from the adipose fat in the skin layer, which matched the PA spectrum of lipid (Figure 2 b). We found that the signal intensities increased by ≈ 7.3 -fold at 1100 nm and ≈ 10.7 -fold at 1300 nm with the injection of $50 \mu\text{L}$ of $40 \mu\text{g mL}^{-1}$ TSPNs (Figure 4a; and Figure S8a, Supporting Information), compared to the signal found in the skin tissue without injection. This significant signal enhancement indicates the capability of TSPN as an exogenous contrast agent for in vivo imaging. In this study, a rat model was adopted, because rat skin has more structural similarities to human tissue than other rodents.^[37,38] However, the density of hair follicles in rat skin is different

from human skin, which means future studies are required to better understand the performance of TSPN for PA imaging in human tissues.

We further evaluated the potential of TSPN for tumor imaging by in vivo PA imaging of TSPNs which were directly injected into PC3-M xenografts in mice (Figure 4b). Without administration of TSPNs, relatively strong PA signals were observed from the tumor tissue only at 800 and 1000 nm, which are attributed to the rich blood vessels surrounding the tumor.^[39–41] Similar to our observation in skin, the signals at 1200 nm are more likely from fats. Then, a $50 \mu\text{L}$ aqueous solution of $40 \mu\text{g mL}^{-1}$ TSPNs was intratumorally injected into the

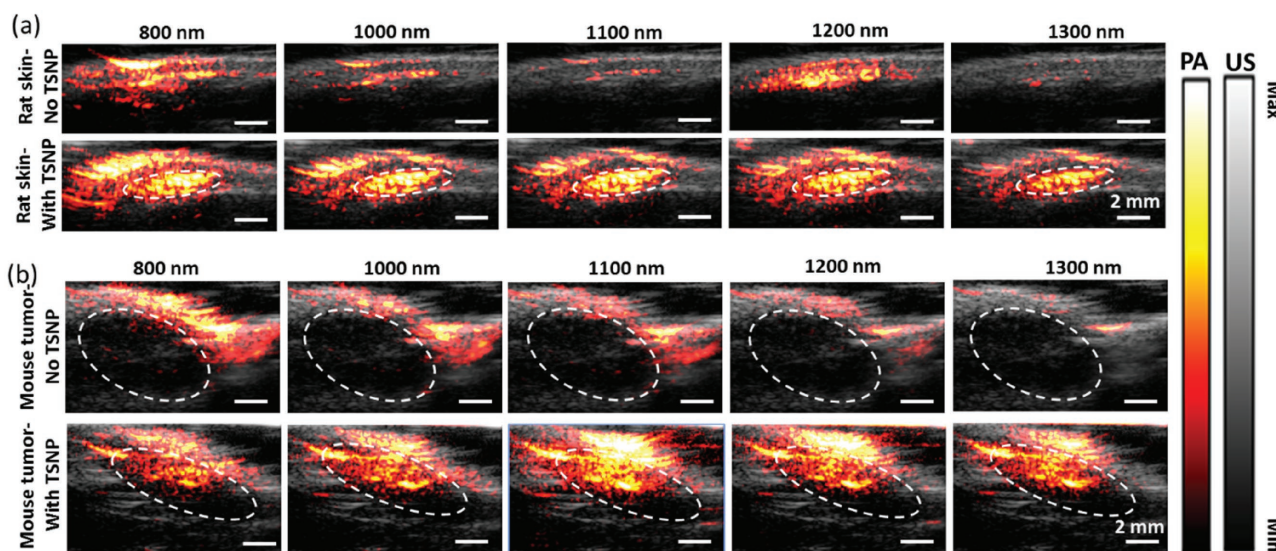


Figure 4. In vivo PA/US imaging of TSPN in rat skin (a) without injection of TSPNs (upper) and with injection of $50 \mu\text{L}$, $40 \mu\text{g mL}^{-1}$ matrigel inclusions of TSPNs (dashed circles) (lower), and in mouse tumor (dashed circles) (b) without injection of TSPNs (upper) and with injection of $50 \mu\text{L}$, $40 \mu\text{g mL}^{-1}$ aqueous solution of TSPNs (lower). The averaged laser energy density was ≈ 10 – 26 mJ cm^{-2} at 800 nm, 19 – 49 mJ cm^{-2} at 1000 nm, 33 – 40 mJ cm^{-2} at 1100 nm, 37 – 46 mJ cm^{-2} at 1200 nm, and 25 – 35 mJ cm^{-2} at 1300 nm. Each image was normalized with the corresponding laser energy density.

tumor (Figure S9, Supporting Information). With the administration of TSPNs, strong PA signals generated within the tumor (dashed circles), with laser excitation wavelengths over 800–1300 nm, respectively. Compared to the images of the tumor without TSPNs, the signal was enhanced ≈ 7.0 -fold at 1100 nm and ≈ 13.3 -fold at 1300 nm (Figure 4b; and Figure S8b, Supporting Information). The overlays between the skin and TSPNs signals might be resulted from the leaking of TSPNs after the injection. Because of the movement of the transducer during the injection of TSPNs, the images (with or without TSPNs) represented the transverse slices of the same tumor at different positions. Moreover, images of fixed mice prostate tumor xenografts before and after injections of TSPNs were recorded to confirm that the signal enhancements were indeed resulted from the introduction of TSPNs, and significant increases in signal were observed after the injections (Figure S10, Supporting Information).

TSPN as a PA contrast agent in NIR-II window was reported. The TSPN is suitable for biological imaging because of its good aqueous stability, nanoscale size, high photostability, and low cytotoxicity. The TSPNs generated a strong PA signal over the entire NIR-II region. The PA spectra and PA imaging in an agar gel phantom reveal that 1100 and 1300 nm are theoretically two optimal wavelengths where the PA signals of two major endogenous contrast agents (lipid and blood) are in the local minima. PA imaging of TSPNs at 1300 nm further benefits from even less intrinsic blood signal from tissue background, while PA imaging at 1100 nm laser might provide higher laser energy on the tissue due to the less light attenuation in water. TSPNs at a comparably low concentration ($40 \mu\text{g mL}^{-1}$) could be readily imaged through a 5.3 cm thick sample of chicken-breast tissues at 1064 nm laser excitation. The potential of TSPN for tumor imaging was demonstrated via intratumoral injection of TSPNs into tumor xenografts. Future functionalization of TSPN with targeting groups promises to establish the utility of TSPN in biomedical imaging.

Experimental Section

Materials and Polymer Synthesis: All reagents were purchased from Sigma-Aldrich and used without further purification unless otherwise noted. Anhydrous *N,N*-dimethylformamide was prepared using an MB-SPS solvent purifying system. TII-TEG was synthesized via palladium-catalyzed C–C cross-coupling techniques and was thoroughly purified to remove any metal residues. The chicken breasts were purchased from a supermarket. Hemoglobin powders were purchased from Sigma-Aldrich. Human whole blood was purchased from Innovative Research (Novi, MI, USA). More details can be found in the Supporting Information.

Synthesis of TSPN: A standard protocol has been developed to prepare SPNs through the nanoprecipitation method. Briefly, a 1 mL THF mixture of TII-TEG (1 mg mL^{-1}) and surfactant DSPE-PEG2000 (2.50 mg mL^{-1}) was rapidly injected into deionized water (9 mL) under continuous sonication with a microtip-equipped probe sonicator (Branson, W-150) at a power output of 6 W for 30 s. After sonication for additional 1 min, THF was removed by nitrogen bubbling. The aqueous solution was filtered through a polyethersulfone (PES) syringe driven filter ($0.45 \mu\text{m}$) and centrifuged three times using a 30 K centrifugal filter unit at 3000 rpm for 3 min at 4°C . The nanoparticle solution was stored in the dark at 4°C .

Characterization: ^1H and ^{13}C NMR spectra were recorded on a Bruker ARX 400 at 293 K with deuterated chloroform as the solvent.

Transmission electron microscopy images were obtained using a Tecnai T20 instrument. DLS was performed using a Malvern Nano-zetasizer. UV/VIS/NIR spectra were recorded with a Cary-6000 system.

Photoacoustic Spectroscopy: The complete description of the photoacoustic spectroscopy setup can be found in elsewhere.^[42] The OPO Laser (EKSPLA NT320) with pulse width 5 ns, repetition rate 10 Hz was applied as excitation laser resource. Nikon Eclipse TE2000-U inverted microscope with a 10 \times objective was used to focus the light to the sample. The laser energy after ND filter was 40–120 μJ . A single-element transducer ($\nu 317\text{-sm}$, 20 MHz) was used to acquire the acoustic and photoacoustic signals. A preamplifier (Olympus 5682, voltage gain 30 dB) and a pulser/receiver (Olympus 5073 pr, ultrasonic bandwidth 75 MHz, voltage gain 39 dB) were used to improve the system sensitivity. All the samples were in the solution state and were sealed in 1 mm-diameter glass tubes. D_2O was applied as the sound coupling agent to avoid water absorption.

Photoacoustic Tomography: The ultrasound and photoacoustic signals were processed by an ultrasound imaging system (Vantage128, Verasonics Inc.). For the penetration study in the chicken-breast tissue a Q-switched Nd:YAG laser (Continuum Surelite SL III-10) with 5 ns pulse with a 10 Hz repetition rate was applied as the laser source. A transmission-mode detection modality was adopted. The laser light was guided to the tissue surface by a fiber bundle and the photoacoustic signals were detected from the other side of the tissue by a low-frequency transducer array (L7-4, PHILIPS/ATL). For the other photoacoustic tomography experiments, the EKSPLA OPO Laser with pulse width 5 ns, repetition rate 10 Hz was applied as excitation laser. In the meantime, a reflection-mode detection was applied with using a customized collinear probe, which has a customized high-frequency ultrasound array (L22-14v, Verasonics Inc.).

Cytotoxicity Test: Cells were cultured in Dulbecco's modified Eagle medium (DMEM) containing 10% fetal bovine serum in a humid environment containing 5% CO_2 and 95% air at 37°C . The in vitro toxicity of different types of human cell lines (A549, HeLa, and Mia PaCa-2) was studied. Cells were first seeded in 96-well plates (3000–5000 cells per well) for, and the culture medium was replaced with fresh medium containing TSPNs at different concentrations ($0\text{--}40 \mu\text{g mL}^{-1}$) and incubated for 24 h. The cell viability was then measured by Cell Counting Kit-8 cytotoxicity array (Dojindo Molecular Technologies, Inc.).

Tumor Mouse Model: PC3-M cells were injected into the prostate of male 6-week-old NSG mice (Purdue University Center for Cancer Research) following protocols reported previously.^[43,44] Tumors were grown for 3 weeks before used for PA tomography imaging. All animal procedures were approved by the Purdue Animal Care and Use Committee.

In Vivo PA Tomography Imaging: All protocols for this experiment were approved by the Purdue Animal Care and Use Committee. NSG mice bearing PC3-M tumor xenografts and 1-month-old healthy Sprague–Dawley rats were anesthetized using 2% isoflurane in oxygen delivered through a nose cone. Prior to photoacoustic imaging, the areas of interest were shaved.

Supporting Information

Supporting Information is available from the Wiley Online Library or from the author.

Acknowledgements

This work was supported by R01HL12385 to J.C. and the Showalter Trust Research Award by Purdue University to J.M.

Conflict of Interest

The authors declare no conflict of interest.

Keywords

contrast agents, deep tissue, near-infrared, photoacoustic imaging, semiconducting polymer nanoparticles

Received: June 18, 2017

Revised: August 4, 2017

Published online:

- [1] R. G. Aswathy, Y. Yoshida, T. Maekawa, D. S. Kumar, *Anal. Bioanal. Chem.* **2010**, 397, 1417.
- [2] G. S. Filonov, A. Krumholz, J. Xia, J. Yao, L. V. Wang, V. V. Verkhusha, *Angew. Chem., Int. Ed.* **2012**, 51, 1448.
- [3] F. Helmchen, W. Denk, *Nat. Methods* **2005**, 2, 932.
- [4] L. V. Wang, S. Hu, *Science* **2012**, 335, 1458.
- [5] L. V. Wang, *Nat. Photonics* **2009**, 3, 503.
- [6] J. Hui, R. Li, E. H. Phillips, C. J. Goergen, M. Sturek, J. X. Cheng, *Photoacoustics* **2016**, 4, 11.
- [7] M. Xu, L. V. Wang, *Rev. Sci. Instrum.* **2006**, 77, 041101.
- [8] L. V. Wang, J. Yao, *Nat. Methods* **2016**, 13, 627.
- [9] Y. Sheng, L. D. Liao, N. Thakor, M. C. Tan, *Sci. Rep.* **2014**, 4, 6562.
- [10] G. Ku, M. Zhou, S. Song, Q. Huang, J. Hazle, C. Li, *ACS Nano* **2012**, 6, 7489.
- [11] Y. Zhou, D. Wang, Y. Zhang, U. Chitgupi, J. Geng, Y. Wang, Y. Zhang, T. R. Cook, J. Xia, J. F. Lovell, *Theranostics* **2016**, 6, 688.
- [12] M. Pramanik, M. Swierczewska, D. Green, B. Sitharaman, L. V. Wang, *J. Biomed. Opt.* **2009**, 14, 034018.
- [13] A. Taruttis, E. Herzog, D. Razansky, V. Ntziachristos, *Opt. Express* **2010**, 18, 19592.
- [14] K. Homan, S. Kim, Y. S. Chen, B. Wang, S. Mallidi, S. Emelianov, *Opt. Lett.* **2010**, 35, 2663.
- [15] K. Welsher, S. P. Sherlock, H. Dai, *Proc. Natl. Acad. Sci. USA* **2011**, 108, 8943.
- [16] L. A. Sordillo, Y. Pu, S. Pratavieira, Y. Budansky, R. R. Alfano, *J. Biomed. Opt.* **2014**, 19, 056004.
- [17] A. M. Smith, M. C. Mancini, S. Nie, *Nat. Nanotechnol.* **2009**, 4, 710.
- [18] K. Pu, N. Chattopadhyay, J. Rao, *J. Controlled Release* **2016**, 240, 312.
- [19] K. Pu, A. J. Shuhendler, J. V. Jokerst, J. Mei, S. S. Gambhir, Z. Bao, J. Rao, *Nat. Nanotechnol.* **2014**, 9, 233.
- [20] K. Pu, J. Mei, J. V. Jokerst, G. Hong, A. L. Antaris, N. Chattopadhyay, A. J. Shuhendler, T. Kurosawa, Y. Zhou, S. S. Gambhir, Z. Bao, J. Rao, *Adv. Mater.* **2015**, 27, 5184.
- [21] K. Pu, A. J. Shuhendler, J. Rao, *Angew. Chem., Int. Ed.* **2013**, 52, 10325.
- [22] J. Zhang, X. Zhen, P. K. Upputuri, M. Pramanik, P. Chen, K. Pu, *Adv. Mater.* **2017**, 29, 1604764.
- [23] Q. Miao, Y. Lyu, D. Ding, K. Pu, *Adv. Mater.* **2016**, 28, 3662.
- [24] Y. Jiang, K. Pu, *Small* **2017**, 13, 1700710.
- [25] Y. Jiang, P. K. Upputuri, C. Xie, Y. Lyu, L. Zhang, Q. Xiong, M. Pramanik, K. Pu, *Nano Lett.* **2017**, 17, 4964.
- [26] Y. Koizumi, M. Ide, A. Saeki, C. Vijayakumar, B. Balan, M. Kawamoto, S. Seki, *Polym. Chem.* **2013**, 4, 484.
- [27] T. Hasegawa, M. Ashizawa, J. Hiyoshi, S. Kawauchi, J. Mei, Z. Bao, H. Matsumoto, *Polym. Chem.* **2016**, 7, 1181.
- [28] G. Ferrauto, F. Carniato, E. Di Gregorio, L. Tei, M. Botta, S. Aime, *Nanoscale* **2017**, 9, 99.
- [29] H. Otsuka, Y. Nagasaki, K. Kataoka, *Adv. Drug Delivery Rev.* **2003**, 55, 403.
- [30] M. Landsman, G. Kwant, G. Mook, W. Zijlstra, *J. Appl. Physiol.* **1976**, 40, 575.
- [31] F. Danhier, O. Feron, V. Preat, *J. Controlled Release* **2010**, 148, 135.
- [32] V. Torchilin, *Adv. Drug Delivery Rev.* **2011**, 63, 131.
- [33] S. Prahl (1998), <http://omlc.ogi.edu/spectra/hemoglobin/index.html>, (accessed: May 2017).
- [34] G. M. Hale, M. R. Querry, *Appl. Opt.* **1973**, 12, 555.
- [35] B. C. Wilson, S. L. Jacques, *IEEE J. Quantum Electron.* **1990**, 26, 2186.
- [36] L. Wang, S. L. Jacques, *J. Opt. Soc. Am. A* **1993**, 10, 1746.
- [37] D. A. Boas, C. Pitris, N. Ramanujam, *Handbook of Biomedical Optics*, CRC Press, Boca Raton, FL, USA, **2011**.
- [38] L. Wang, S. L. Jacques, L. Zheng, *Comput. Methods Programs Biomed.* **1995**, 47, 131.
- [39] G. M. El Maghraby, B. W. Barry, A. C. Williams, *Eur. J. Pharm. Sci.* **2008**, 34, 203.
- [40] R. C. Wester, H. I. Maibach, *J. Toxicol., Cutaneous Ocul. Toxicol.* **2001**, 20, 411.
- [41] J. Folkman, *N. Engl. J. Med.* **1971**, 285, 1182.
- [42] J. Folkman, *J. Natl. Cancer Inst.* **1990**, 82, 4.
- [43] A. De la Zerde, C. Zavaleta, S. Keren, S. Vaithilingam, S. Bodapati, Z. Liu, J. Levi, B. R. Smith, T. J. Ma, O. Oralkan, Z. Cheng, X. Chen, H. Dai, B. T. Khuri-Yakub, S. S. Gambhir, *Nat. Nanotechnol.* **2008**, 3, 557.
- [44] H. W. Wang, N. Chai, P. Wang, S. Hu, W. Dou, D. Umulis, L. V. Wang, M. Sturek, R. Lucht, J. X. Cheng, *Phys. Rev. Lett.* **2011**, 106, 238106.
- [45] J. Pavese, I. M. Ogden, R. C. Bergan, *J. Vis. Exp.* **2013**, e50873.
- [46] S. I. Park, S. J. Kim, L. K. McCauley, G. E. Gallick, *Curr. Protoc. Pharmacol.* **2010**, 14,15.
- [47] X. X. Chen, Z. J. Zhang, Z. C. Ding, J. Liu, L. X. Wang, *Angew. Chem., Int. Ed.* **2016**, 55, 10376.